Dispersion management for controlling image plane in Fourier-domain spectrally encoded endoscopy

Michal Merman and Dvir Yelin*

Department of Biomedical Engineering, Technion – Israel Institute of Technology, Technion City 32000, Haifa, Israel
*yelin@bm.technion.ac.il

Abstract: Spectrally encoded endoscopy (SEE) uses single optical fiber and miniature diffractive optics to allow imaging through a miniature probe. Utilizing Fourier-domain interferometry, SEE was shown capable of video-rate three-dimensional imaging, albeit at limited depth of field due to the limited spectral resolution of the detection spectrometer. We show that by using dispersion management at the reference arm of the interferometer, the tilt and curvature of the field of view could be adjusted without modifying the endoscopic probe itself. By controlling the group velocity dispersion, this technique is demonstrated useful for imaging specimen regions which reside outside the system's depth of field. This approach could be used to improve usability, functionality and image quality of SEE without affecting probe size and flexibility.

OCIS codes: (170.2150) Endoscopic imaging; (110.3175) Interferometric imaging; (260.2030) Dispersion; (320.1590) Chirping; (110.6880) Three-dimensional image acquisition.

References and links

1. J. Knittel, L. Schnieder, G. Buess, B. Messerschmidt, and T. Possner, "Endoscope-compatible confocal microscope using a gradient index-lens system," Opt. Commun. **188**(5-6), 267–273 (2001).
2. Y. S. Sabharwal, A. R. Rouse, L. Donaldson, M. F. Hopkins, and A. F. Gmitro, "Slit-scanning confocal microendoscope for high-resolution in vivo imaging," Appl. Opt. **38**(34), 7133–7144 (1999).
3. H. Schoffl, S. M. Froschauer, R. Hainisch, D. Hager, R. Schnelzer, O. Kwasny, and G. M. Huemer, "Intraluminal endoscopic evaluation of microvascular anastomosis," J. Plast. Reconstr. Aesthet. Surg. **61**(4), 388–392 (2008).
4. J. T. Sun, C. H. Shu, B. Appiah, and R. Drezek, "Needle-compatible single fiber bundle image guide reflectance endoscope," J. Biomed. Opt. **15**(4), 040502 (2010).
5. C. M. Brown, P. G. Reinhall, S. Karasawa, and E. J. Seibel, "Optomechanical design and fabrication of resonant microscanners for a scanning fiber endoscope," Opt. Eng. **45**(4), 043001–043010 (2006).
6. D. L. Dickensheets, and G. S. Kino, "Micromachined scanning confocal optical microscope," Opt. Lett. **21**(10), 764–766 (1996).
7. C. M. Lee, C. J. Engelbrecht, T. D. Soper, F. Helmchen, and E. J. Seibel, "Scanning fiber endoscopy with highly flexible, 1 mm catheterscopes for wide-field, full-color imaging," J Biophotonics **3**(5-6), 385–407 (2010).
8. G. J. Tearney, M. Shishkov, and B. E. Bouma, "Spectrally encoded miniature endoscopy," Opt. Lett. **27**(6), 412–414 (2002).
9. D. Yelin, I. Rizvi, W. M. White, J. T. Motz, T. Hasan, B. E. Bouma, and G. J. Tearney, "Three-dimensional miniature endoscopy," Nature **443**(7113), 765–765 (2006).
10. D. Yelin, W. M. White, J. T. Motz, S. H. Yun, B. E. Bouma, and G. J. Tearney, "Spectral-domain spectrally-encoded endoscopy," Opt. Express **15**(5), 2432–2444 (2007).
11. D. Yelin, B. E. Bouma, and G. J. Tearney, "Volumetric sub-surface imaging using spectrally encoded endoscopy," Opt. Express **16**(3), 1748–1757 (2008).
12. D. Yelin, B. E. Bouma, J. J. Rosowsky, and G. J. Tearney, "Doppler imaging using spectrally-encoded endoscopy," Opt. Express **16**(19), 14836–14844 (2008).
13. R. Leitgeb, C. Hitzenberger, and A. Fercher, "Performance of fourier domain vs. time domain optical coherence tomography," Opt. Express **11**(8), 889–894 (2003).
14. M. Merman, A. Abramov, and D. Yelin, "Theoretical analysis of spectrally encoded endoscopy," Opt. Express **17**(26), 24045–24059 (2009).
15. G. J. Tearney, B. E. Bouma, and J. G. Fujimoto, "High-speed phase- and group-delay scanning with a grating-based phase control delay line," Opt. Lett. **22**(23), 1811–1813 (1997).
16. C. H. Brito Cruz, P. C. Becker, R. L. Fork, and C. V. Shank, "Phase correction of femtosecond optical pulses using a combination of prisms and gratings," Opt. Lett. **13**(2), 123–125 (1988).

#138356 - $15.00 USD Received 18 Nov 2010; revised 7 Feb 2011; accepted 7 Feb 2011; published 25 Feb 2011

17. R. L. Fork, O. E. Martinez, and J. P. Gordon, "Negative dispersion using pairs of prisms," Opt. Lett. **9**(5), 150–152 (1984).
18. O. E. Martinez, J. P. Gordon, and R. L. Fork, "Negative group-velocity dispersion using refraction," J. Opt. Soc. Am. A **1**(10), 1003–1006 (1984).
19. E. Treacy, "Optical pulse compression with diffraction gratings," IEEE J. Quantum Electron. **5**(9), 454–458 (1969).
20. D. Yelin, S. H. Yun, B. E. Bouma, and G. J. Tearney, "Three-dimensional imaging using spectral encoding heterodyne interferometry," Opt. Lett. **30**(14), 1794–1796 (2005).

1. Introduction

Despite a number of image quality issues, sub-millimeter diameter endoscopes have been shown useful for clinical applications that require minimally invasive diagnosis with low tissue damage. Fiber bundle endoscopes, which are most commonly used for such applications, frequently suffer from low fiber count, high fiber cross-talk, and pronounced image artifacts caused by the dark gaps between the fibers [1–4]. Single fiber endoscopes that employ miniature distal mechanical scanning often provide higher image quality; however, their imaging speed is limited by the speed and accuracy of the scanning apparatus [5–7]. Recently, a method termed spectrally-encoded endoscopy (SEE) [8,9] was introduced, utilizing a single optical fiber and miniature diffractive optics to encode transverse reflections from a sample. Since rapid lateral scanning is not required in this approach, SEE is capable of high quality imaging through ultra-miniature, flexible, single fiber endoscopic probes. Using low coherence Fourier-domain interferometry, recent works have demonstrated that SEE is capable of video rate, three-dimensional imaging of surface [9,10] and subsurface [11] tissue structures, as well as Doppler imaging of acoustic vibrations and flow [12]. In addition to providing depth information for three-dimensional visualization of a specimen, Fourier-domain interferometry allows heterodyne signal detection scheme which greatly improves signal-to-noise ratio, enabling fast and efficient low numerical aperture (NA) imaging of scattering targets [10].

While the lateral field of view of Fourier-domain SEE is governed by the groove density of the diffraction grating and by the focal length of its lens, and could be made sufficiently large with adequate probe design, the axial field of view ("depth of field") depends on the overlap between the confocal parameter of the lens and the coherence gating of the system. In small diameter probes, the confocal range is large, resulting with depth of field that is limited by the spectral resolution of the detection system. This resolution limit results in a sensitivity falloff caused by the decreased contrast at high frequency spectral interference fringes [13]. For example, for an SEE probe with 1800 lines/mm grating, 10 mm focal length and 250 nm source bandwidth, the lateral field of view is approximately [14] 6.3 x 6.3 mm, but the axial field of view (6 dB sensitivity falloff, full width), assuming spectrometer resolution of 0.1 nm, is only 2.8 mm. Tissue structures with steep depth profiles such as the middle ear ossicles, would require stepping the reference mirror and acquiring multiple images to generate an extended depth view [10], or would otherwise be impossible to image at high frame rates.

Another difficulty that is associated with the field of view of SEE is related to its steep angle with respect to the main probe axis [9] (twice the grating Littrow's angle [14]). In some potential clinical applications of SEE, such as in small ducts or in small spaces (e.g. the middle ear) where probe steering is limited, this angle would severely affect the field of view and deteriorate image quality.

In this paper we address the challenge of the limited field of view by controlling the spectral phase difference between the probe and reference arms. We show that group velocity dispersion difference between the two interferometer arms directly affects the angle between the image plane and the probe axis, with practically no side effects on image quality. By allowing the adjustment of the field of view from outside the patient body, this technique enables the endoscopist to image tissue parts even in the most hard-to-reach parts of the body, without adding to the complexity and the bulk of the endoscopic probe.

#138356 - $15.00 USD Received 18 Nov 2010; revised 7 Feb 2011; accepted 7 Feb 2011; published 25 Feb 2011

2. Theory

A Fourier-domain SEE system [11] captures the spectral interference between the spectrally encoded image and a reference signal. Data processing in Fourier-domain SEE is performed using windowed Fourier transforms, where each spectral window corresponds to the bandwidth of a single resolvable point on the sample. The modulation frequency (in the ω axis) of the interference signal, for a single resolution element illuminated by a narrow spectral band centered at ω_m, is linearly proportional to the difference in group delay τ between the interferometer arms: $\tau(\omega_m) = \tau_s(\omega_m) - \tau_r(\omega_m)$, where τ_s and τ_r denote the group delay at the sample and reference arms, respectively. The local group delay difference could be also expressed by first derivative of the spectral phase difference $\varphi(\omega)$ between the interferometer arms:

$$\tau(\omega_m) = \left.\frac{d\varphi(\omega)}{d\omega}\right|_{\omega_m} = \frac{z(\omega_m)}{c}, \tag{1}$$

where $z(\omega_m) = z_s(\omega_m) - z_r(\omega_m)$ denotes the optical path difference for ω_m between the sample (z_s) and the reference (z_r) optical paths, and c denotes the speed of light.

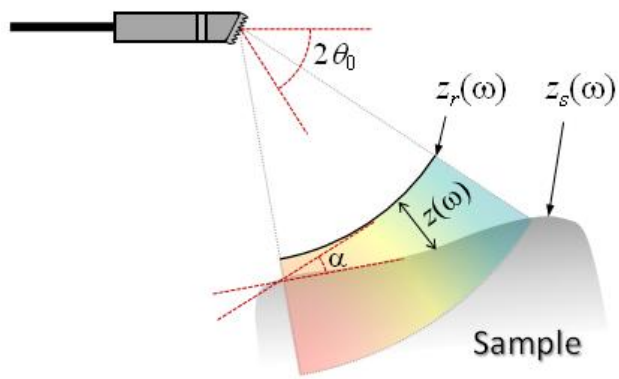

Fig. 1. Schematic illustration of the relative sample and reference optical paths. Here, the reference path length z_r is assumed to be equal for all ω's.

An arbitrary surface whose axial position relative to the reference plane is denoted by $z(\omega)$, is schematically illustrated in Fig. 1. Assuming that the surface is smooth (on a wavelength scale) and continuous, the axial location of the point encoded by ω_m could be represented by a Taylor series around the center angular frequency of the entire spectrum ω_0:

$$z(\omega_m) = z(\omega_0) + \left.\frac{dz}{d\omega}\right|_{\omega_0}(\omega_m - \omega_0) + \frac{1}{2}\left.\frac{d^2 z}{d\omega^2}\right|_{\omega_0}(\omega_m - \omega_0)^2 + \ldots\ , \tag{2}$$

where the first derivative at ω_0 corresponds to a linear tilt of the sample relative to the reference plane (with a tilt angle α), and the second derivative at ω_0 represents a relative parabolic curvature.

Similarly, the spectral phase difference $\varphi(\omega)$ at each point along the spectrally encoded line could also be represented by a Taylor series around the center angular frequency:

$$\varphi(\omega) = \varphi_0 + \left.\frac{d\varphi(\omega)}{d\omega}\right|_{\omega_0}(\omega - \omega_0) + \frac{1}{2}\left.\frac{d^2\varphi(\omega)}{d\omega^2}\right|_{\omega_0}(\omega - \omega_0)^2 + \frac{1}{6}\left.\frac{d^3\varphi(\omega)}{d\omega^3}\right|_{\omega_0}(\omega - \omega_0)^3 + \ldots\ . \tag{3}$$

#138356 - $15.00 USD Received 18 Nov 2010; revised 7 Feb 2011; accepted 7 Feb 2011; published 25 Feb 2011

By substituting Eq. (2) and Eq. (3) into Eq. (1), and calculating the derivative in Eq. (1), we obtain:

$$c\left.\frac{d\varphi}{d\omega}\right|_{\omega_0}+c\left.\frac{d^2\varphi}{d\omega^2}\right|_{\omega_0}\left(\omega_m-\omega_0\right)+\frac{c}{2}\left.\frac{d^3\varphi}{d\omega^3}\right|_{\omega_0}\left(\omega_m-\omega_0\right)^2+\ldots=$$
$$=z\left(\omega_0\right)+\left.\frac{dz}{d\omega}\right|_{\omega_0}\left(\omega_m-\omega_0\right)+\frac{1}{2}\left.\frac{d^2z}{d\omega^2}\right|_{\omega_0}\left(\omega_m-\omega_0\right)^2+\ldots\ . \tag{4}$$

The identity in Eq. (4) would be true for every ω_m only if all the coefficients of the corresponding powers of ω_m were equal:

$$z\left(\omega_0\right)=c\left.\frac{d\varphi\left(\omega\right)}{d\omega}\right|_{\omega_0}, \tag{5}$$

$$\left.\frac{dz}{d\omega}\right|_{\omega_0}=c\left.\frac{d^2\varphi\left(\omega\right)}{d\omega^2}\right|_{\omega_0}, \tag{6}$$

and

$$\left.\frac{d^2z}{d\omega^2}\right|_{\omega_0}=c\left.\frac{d^3\varphi\left(\omega\right)}{d\omega^3}\right|_{\omega_0}. \tag{7}$$

Equations (5)-(7) imply that the effective image plane in the sample arm of SEE could be controlled by manipulating the relative spectral phases. To maintain simplicity of the sample arm, phase adjustments could be conveniently applied at the reference arm using a tunable optical arrangement. With zero differences in the high order spectral phase derivatives (no dispersion difference), the imaging plane at the sample arm could be adjusted to match the sample height at the center frequency (Eq. (5)) according to: $z_s\left(\omega_0\right)=z_r\left(\omega_0\right)+c\left[d\varphi/d\omega\right]_{\omega_0}$. Hence, the axial location of the imaging plane could be controlled either by adjusting the optical path delay at the reference arm $z_r(\omega_0)$ [9–11], and/or by adjusting the linear term of the spectral phase, for example by using a rapid scanning optical delay line (RSOD) [15].

Adjusting the field of view of SEE for imaging angled surfaces would be necessary for many applications where probe navigation is relatively limited. In order to derive an explicit expression which relates tilt of the field of view to the second order phase derivative, also termed group velocity dispersion (GVD), we first use the equation which approximates the angular frequency interval $\delta\omega$ to spatial interval δx [14]:

$$\delta x\cong-\frac{2\pi z_0Gc}{\omega^2\cos\theta}\delta\omega, \tag{8}$$

where z_0 denotes the sample distance from the grating for the central wavelength, G denotes the groove density of the probe grating and θ denotes the diffraction angle. Using the identity $dz/d\omega=\left(dz/dx\right)\cdot\left(dx/d\omega\right)$ and substituting the result in Eq. (6) we finally obtain:

$$\left.\frac{d^2\varphi\left(\omega\right)}{d\omega^2}\right|_{\omega_0}=-\frac{2\pi Gz_0}{\cos\theta_0\omega_0^{\ 2}}\tan\alpha\ , \tag{9}$$

where θ_0 denotes the Littrow's angle for ω_0 and α denotes the tilt angle of the field of view, as shown in Fig. 1. Note that positive values of α correspond to image plane tilts which lead to shorter optical paths for angular frequencies (wavelengths) higher (shorter) than the central angular frequency (wavelength).

#138356 - $15.00 USD Received 18 Nov 2010; revised 7 Feb 2011; accepted 7 Feb 2011; published 25 Feb 2011

Higher order terms in Eq. (4) relate the higher order derivatives of $\varphi(\omega)$ and $z(\omega)$, however their practical effect is less crucial for current SEE system parameters. Using specifically tailored dispersion management, one could compensate for the inherent field curvature (see the curved reference plane in Fig. 1) by introducing a negative third order derivative at the reference spectral phase, according to Eq. (7).

3. Experimental imaging system

Our benchtop spectrally encoded imaging system (Fig. 2) consisted of a broadband titanium sapphire oscillator (Femtolasers Rainbow, 300 nm bandwidth, 800 nm center wavelength) coupled to a 50/50 single-mode optical fiber (numerical aperture approx. 0.12) coupler within a Michelson interferometer arrangement. The sample arm consisted of a fiber collimator (11 mm effective focal length), a focusing lens (40 mm focal length) and a 1200 lines/mm transmission diffraction grating (G), with 30° Littrow's angle at 830 nm. The distance (z_0) from the grating to the sample was approximately 35 mm. The spectral line was scanned in the y axis by a galvanometric scanner (6220HB, Cambridge Technology Inc.) which was placed between the grating and the sample (not shown in Fig. 2 for brevity). The reference arm consisted of a collimating lens, a variable neutral density (ND) filter, a dispersion control unit, and a mirror mounted on a translation stage. Interferograms of the reflected spectra from the sample and the reference arms were detected by a custom spectrometer, comprised of a collimating lens (50 mm focal length), an 1800 lines/mm transmission diffraction grating, a focusing lens (Nikon, AF Nikkor 85 mm focal length) and a high-speed line camera (Basler Sprint spL4096).

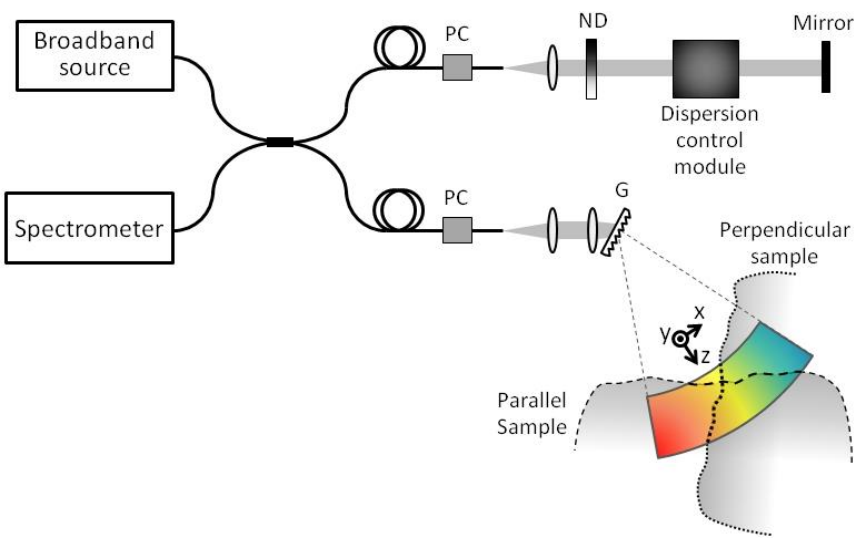

Fig. 2. A schematic of the Fourier domain spectrally encoded imaging system. The effective cross-sectional imaging range without dispersion difference between the two arms is marked by the color gradient area. Two examples for possible sample orientations are shown: a nearly parallel sample (surface marked by dashed line) and a nearly perpendicular sample (dotted surface). Thick dotted and dashed lines correspond to the surface regions that could be imaged with the uncorrected field of view. PC – polarization controller, G – diffraction grating, ND – neutral density filter.

Shown in Fig. 2 are two examples for sample orientations relative to the cross-sectional field of view of the system without dispersion compensation (marked by a color gradient). Note that only part of the surface of the sample which is parallel to the probe axis (surface marked by a dashed curve) could be imaged. Similarly, a sample whose surface lies perpendicular to the probe axis (surface marked by dotted curve) would also be only partly imaged.

#138356 - $15.00 USD Received 18 Nov 2010; revised 7 Feb 2011; accepted 7 Feb 2011; published 25 Feb 2011

4. Results

4.1 Imaging a surface parallel to the probe axis

In applications that require insertion of the SEE probe into tubular structures such as blood vessels and small ducts, the tissue surface of interest would often lie in parallel to the probe axis. The negative angle between the probe and the sample surface could be corrected by introducing a positive GVD at the reference arm (see Eq. (9)), for example, by adding a fiber of length l_d. The second derivative of the spectral phase difference is then given by:

$$\left.\frac{d^2\varphi(\omega)}{d\omega^2}\right|_{\omega_0} = k''(\omega_0)\, l_d, \tag{10}$$

where k'' denotes the second derivative of the angular wavenumber with respect to ω (a property of the silica fiber itself).

In order to demonstrate the adjustment of the field of view for optimizing visibility of a sample plane parallel to the probe axis, a USAF 1951 scattering resolution test target was positioned at an angle of −4° with respect to the main optical axis, corresponding to approximately α = -38° tilt of the sample relative to the uncorrected imaging plane. The imaged area on the sample was approximately 9 mm in the *x* (wavelength) axis and 4 mm in the *y* axis. Imaging rate was 8 frames per second. With no dispersion difference between the sample and reference arms, more than half of the field of view was barely visible (Fig. 3a). Adding a 62 cm long silica fiber to the reference arm and matching the optical path lengths between the two interferometer arms, the field of view was tilted by approximately 22° toward the sample plane, resulting with a full coverage of the sample surface with full depth information throughout the image (Fig. 3b).

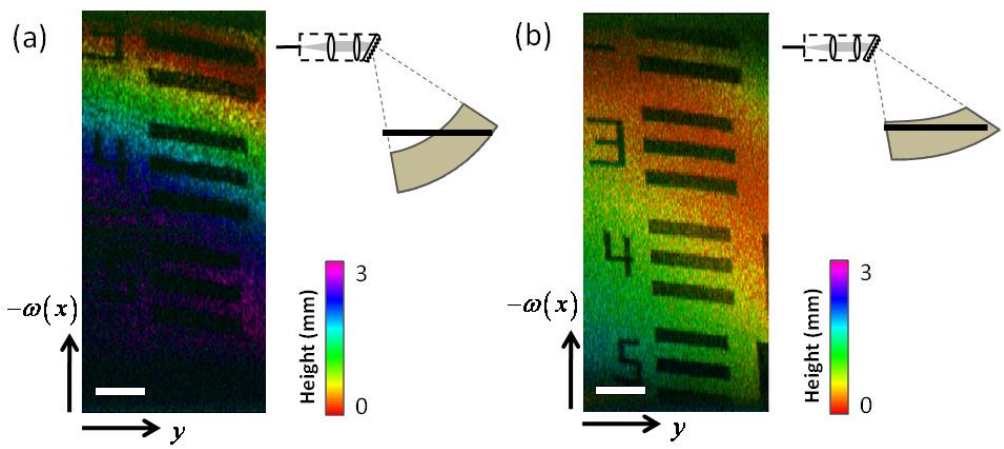

Fig. 3. Images of a portion of a resolution target acquired by Fourier-domain spectrally encoded imaging, with the target positioned in parallel to probe axis (a) before and (b) after the addition of 62 cm fiber in the reference arm. Images are presented using a logarithmic look-up table. Scale bars represent 1 mm. Schematic illustrations of the relative positions of the probe, the field of view and the target (represented by straight black line) are shown adjacent to the images.

4.2 Imaging a sample perpendicular to the probe axis

Imaging samples which face perpendicular to the SEE probe requires the reference arm to have lower GVD than the sample arm. Negative GVD is commonly induced by using combinations of prism and grating pairs [16–19]. The second order derivative of the spectral phase φ_{GP}, induced by a chirp filter comprised of a pair of identical diffraction gratings, is given by [19]:

#138356 - $15.00 USD Received 18 Nov 2010; revised 7 Feb 2011; accepted 7 Feb 2011; published 25 Feb 2011

$$\left.\frac{d^2\varphi_{GP}(\omega)}{d\omega^2}\right|_{\omega_0} = -\frac{4\pi^2 c G'^2 b}{\omega_0^{\,3}\cos^3\theta'} \tag{11}$$

where b denotes the perpendicular distance between the gratings, G' denotes the gratings' groove density and θ' denotes the Littrow's angle at the center angular frequency ω_0.

In order to demonstrate SEE imaging of a sample perpendicular to the probe axis, the USAF 1951 resolution test target was positioned approximately 86° with respect to the probe axis, corresponding to α = 52° angle with the reference plane with zero dispersion difference (Fig. 4). Transmission gratings with 1200 lines/mm were used, separated by approximately 30 mm, which resulted with a field of view tilt by 48°. Comparing the SEE images of the resolution target with zero dispersion difference (Fig. 4a), and with approx. 60,000 fs^2 dispersion at the reference arm (Fig. 4b), reveals significant improvement in field of view.

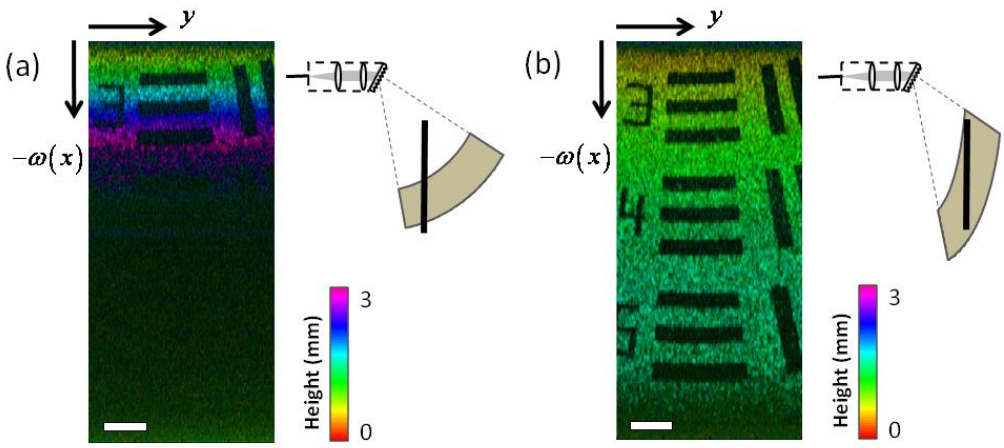

Fig. 4. Images of a portion of a resolution target acquired by Fourier-domain spectrally encoded imaging, with the target positioned perpendicular to main optical axis (a) before and (b) after the introduction of negative GVD at the reference arm. Images are presented using a logarithmic look-up table. Scale bars represent 1 mm. Schematic illustrations of the relative positions of the probe, the field of view and the target (represented by straight black line) are shown adjacent to the images.

One potential application of SEE is the visualization of the middle ear ossicles in patients with hearing disorders. Thanks to its small diameter probe [9] and its ability to record three-dimensional images of acoustic vibrations [12] Fourier-domain SEE would be capable to conduct functional imaging with minimum tissue damage. Since probe steering inside the middle ear would be extremely challenging and unsafe, the limited depth of field of Fourier-domain SEE may limit the value of the endoscopic procedure. In order to demonstrate effective three-dimensional imaging of a middle ear ossicle without moving the probe, a bovine stapes was attached to a flat surface (Fig. 5). When an endoscopic probe is inserted into the middle ear through the Eustachian tube, its axis would be nearly perpendicular to the main axis of the stapes which spans along its head, the two crura, and the foot plate. To simulate such configuration, we have imaged the stapes at approximately 90° angle between the probe and the stapes main axis, in a similar configuration as in Fig. 4. With no GVD difference between the interferometer arms, the foot plate could be clearly observed (Fig. 5a), however the two crura, the neck and the head of the stapes, all fall outside the image range and appear dark. With a grating pair separated by 30 mm in the reference arm, the stapes could be fully visualized (Fig. 5b), while maintaining the same view angle between the probe and the ossicle. The dark horizontal lines on the flat surface below the stapes in Fig. 5a-b correspond to the reference plane which results with no spectral modulation, and was filtered out by our data processing algorithms.

#138356 - $15.00 USD Received 18 Nov 2010; revised 7 Feb 2011; accepted 7 Feb 2011; published 25 Feb 2011

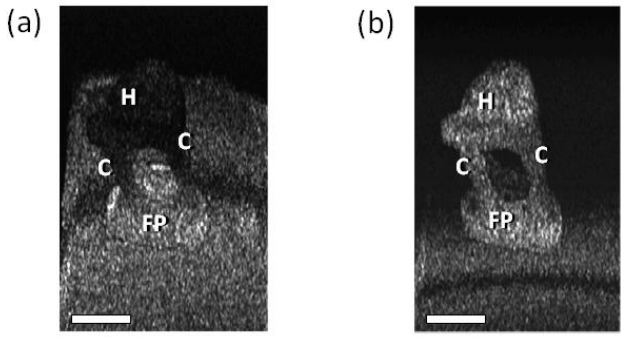

Fig. 5. Images of a bovine stapes acquired by Fourier domain spectrally encoded imaging. The reflectivity image is shown (a) without image plane correction and (b) after image plane correction using a negative GVD filter at the reference arm. Scale bars represent 1 mm. FP – foot plate, C - crus, H – head.

5. Discussion

Due to the small bandwidth illuminating each point on a sample in SEE [14], dispersion often has insignificant effect on axial resolution, in contrast, for example, with most optical coherence tomography (OCT) applications. Therefore, spectral phases may be used to control imaging parameters without compromising image quality. Moreover, phase adjustments could be accomplished outside the patient using only the reference arm of the interferometer, without compromising the simplicity and small dimensions of the imaging probe.

While a plane mirror on a translation stage would be sufficient to control the axial location of the image, a more sophisticated dispersion control module would provide GVD adjustment to control image tilt, or second order GVD to control image curvature. Such control would increase the SNR by allowing high contrast in the spectral modulation fringes, improving image quality and uniformity across the field of view.

In any practical implementation of the new technique presented in this work, some challenges still exist in the system's optical design and user interface. First, the depth of field is fundamentally limited by the depth of focus of the imaging lens, which could range from approximately 6 mm for ultra-thin probes (250 μm diameter), down to a few hundreds of microns for 1 mm diameter probes. In comparison, practical Fourier domain SEE systems would have interferometric field depths of 1-2 millimeters, depending primarily on the spectrometer resolution. Consequently, controlling the axial field of view by dispersion management would be effective for thin, sub-millimeter probes with small numerical apertures (<0.02), whose field of view is limited only by interferometry. Second, independent, real-time control over the sign and magnitude of the different orders of the spectral phase is difficult to implement experimentally, and would be less realistic for a practical SEE system. A feasible solution to this problem would be to adjust the image angle using GVD only, and to compensate for higher order image plane aberrations by post-processing the data. Alternatively, two or more preset optical components with known GVD values could be utilized to rapidly switch between different view angles, which could reduce system complexity and improve user interface. Evidently, there is a limit to the amount of sample tilts that could be effectively compensated without moving the probe, and without deteriorating both axial and lateral resolutions. For example, assuming probe focal length of 10 mm, tilting the field of view by $\alpha = 60°$ would require GVD of approximately 40,000 fs^2, which would reduce axial resolution by approximately 35% (assuming spectral resolution of 2 nm) and deteriorate lateral resolution by a factor of two. Finally, the introduction of positive GVD at the reference arm using a dispersive optical fiber (Section 4.1), would be difficult to implement in simple SEE system and probe, since the excess path length cannot be independently compensated for in a fixed length probe. Possible solutions to this challenge include the addition of a delay line at the sample arm outside the patient body, or,

#138356 - $15.00 USD Received 18 Nov 2010; revised 7 Feb 2011; accepted 7 Feb 2011; published 25 Feb 2011

alternatively by adding an RSOD [20] to the reference arm for inducing negative linear spectral phase to compensate for the physical path length induced by the fiber.

In summary, we have formulated and demonstrated new means for adjusting the imaging plane in Fourier-domain SEE. Using dispersion management at the reference arm, the technique was demonstrated useful for increasing the field of view on a resolution test target and a bovine ear bone, which were placed at large angles with respect to the original, uncorrected field of view. In a future clinical SEE system, dispersion control could be accomplished in real time, allowing the endoscopist to capture the best possible images even in the most hard-to-reach parts of the body, with short procedure times and minimal probe navigation.

Acknowledgements

The study was funded in part by the Israel Science Foundation grant (716/09) and by the European Research Council starting grant (239986).

#138356 - $15.00 USD Received 18 Nov 2010; revised 7 Feb 2011; accepted 7 Feb 2011; published 25 Feb 2011